

Solving the inverse problem of high numerical aperture focusing using Slepian-type vector fields

Kornél Jahn*, Nándor Bokor

Department of Physics, Budapest University of Technology and Economics, 1111 Budapest, Budafoki út 8., Hungary

Abstract

A technique using vector Slepian harmonics and multipole fields is presented for a general treatment of the inverse problem of high numerical aperture focusing. A prescribed intensity distribution or electric field distribution in the focal volume is approximated using numerical optimization and the corresponding illuminating field at the entrance pupil is constructed. As illustrations, three examples, the optical needle, tube, and bubble are considered.

Keywords: High numerical aperture focusing, Vector diffraction theory, Inverse problem, Slepian's concentration problem

1. Introduction

Engineering the focal spot of a high numerical aperture (NA) lens is a central problem in several optical applications such as laser scanning microscopy, optical trapping and laser micromachining. To obtain the desired spot, one usually has to solve a numerical optimization problem. There have been several examples of the design of annular amplitude or phase masks for an input beam with a given amplitude profile and polarization state [1–4]. These calculations usually rely on the Debye–Wolf diffraction integral [5] for determining the focused field.

Instead of the direct numerical evaluation of the Debye–Wolf integral, some methods use analytical series expansions such as the multipole theory of focusing [6], the technique of Kant using Gegenbauer polynomials and spherical Bessel functions [7], the extended Nijboer–Zernike approach [8] or the scalar eigenfunction expansion of Sherif et al. using Slepian's prolate spheroidal functions [9]. Some of these methods were also used for solving the inverse problem of focusing [10–12]. Recently, a technique using dipole arrays has also been proposed [13, 14].

All the methods above, however, possess some inherent drawbacks: they are either applicable component-wise only [10, 12], lack directionality [6], are generally computationally challenging [11] or are tailored for a specific problem [13, 14].

Based on the multipole theory of focusing [6], we recently proposed the orthonormal basis of vector Slepian harmonics (VSLHs) which are naturally suitable for approximating the illumination in a high NA system [15]. Its main advantage is that a subset exhibits excellent directionality, i.e. its angular energy distribution is confined to the solid angle of illumination. Each VSLH basis function represents the angular spectrum of a focused field described by a corresponding vector Slepian multipole field (VSLMF). The directionality of the VSLHs allows

us to approximate common illumination angular spectra using a smaller number of coefficients than a representation using the vector spherical harmonics [15].

In this paper, we demonstrate the applicability of these novel vector bases for general inverse problems in high NA focusing. As illustrations, three examples are considered: the optical needle [13], tube [14] and bubble [4] focal spots.

2. The theory of vector Slepian bases

First we give a brief introduction to the new vector Slepian bases discussed more comprehensively in Ref. [15]. One can approximate a divergence-free, monochromatic focused electric field satisfying the vector Helmholtz equation as

$$\mathbf{E}(\mathbf{r}) = \sum_m \sum_{i=1}^{i_{\max}} c_{mi} \mathbf{\Phi}_{mi}(\mathbf{r}), \quad (1)$$

where the vector functions $\mathbf{\Phi}_{mi}(\mathbf{r})$ are the VSLMFs and c_{mi} denote complex expansion coefficients (determined in this paper by numerical optimization, as discussed in Section 3). The VSLMFs themselves are linear combinations of a finite number of vector multipole fields (VMFs) $\mathbf{M}_{lm}(\mathbf{r})$ and $\mathbf{N}_{lm}(\mathbf{r})$ [15] of the same order m , i.e.

$$\mathbf{\Phi}_{mi}(\mathbf{r}) := \sum_{l=\ell_m}^L [u_{ilm} \mathbf{M}_{lm}(\mathbf{r}) + v_{ilm} \mathbf{N}_{lm}(\mathbf{r})], \quad (2)$$

where L denotes the maximal degree of the contributing VMFs and the summation starts at

$$\ell_m := \begin{cases} 1 & \text{if } m = 0 \\ |m| & \text{otherwise} \end{cases}.$$

On the calculation of the coefficients u_{ilm} and v_{ilm} of Eq. (2), we refer to Ref. [15].

*Corresponding author

Email address: kornel.jahn@gmail.com (Kornél Jahn)

The azimuthal properties of $\Phi_{mi}(\mathbf{r})$ are solely determined by the order m . In most cases, only VSLMFs of certain values of m contribute to the focused field, e.g. for focused fields of linearly or circularly polarized input beams or cylindrical vector beams. The second integer index i indexes VSLMFs of the same order m , however, the limit i_{\max} of Eq. (1) is usually chosen much less than the number N_m of available VSLMFs for a given order m , where

$$N_m := \begin{cases} L & \text{if } m = 0 \\ L - |m| + 1 & \text{otherwise} \end{cases} . \quad (3)$$

To clarify the reason of this choice, we must first recall the plane-wave representation of these fields.

The VSLMFs can also be expressed as a superposition of elementary plane-waves, i.e.

$$\Phi_{mi}(\mathbf{r}) = \frac{ik}{2\pi} \int_0^{2\pi} \int_0^\pi \mathbf{U}_{mi}(\theta_s, \phi_s) \exp(-ik\hat{\mathbf{s}} \cdot \mathbf{r}) \sin \theta_s d\theta_s d\phi_s, \quad (4)$$

where $k = 2\pi/\lambda$ denotes the wavenumber (λ is the wavelength), θ_s and ϕ_s are angular spherical coordinates, $\hat{\mathbf{s}} = \sin \theta_s \cos \phi_s \hat{\mathbf{e}}_x + \sin \theta_s \sin \phi_s \hat{\mathbf{e}}_y + \cos \theta_s \hat{\mathbf{e}}_z$ is the propagation unit vector of a plane-wave component with an amplitude and polarization specified by the vector angular spectrum $\mathbf{U}_{mi}(\theta_s, \phi_s)$ and the transversality relation $\mathbf{U}_{mi}(\theta_s, \phi_s) \cdot \hat{\mathbf{s}} = 0$ holds.

Analogously to Eq. (2), the functions $\mathbf{U}_{mi}(\theta, \phi)$ are also defined as a linear combination:

$$\mathbf{U}_{mi}(\theta, \phi) := \sum_{l=\ell_m}^L [u_{ilm} \mathbf{Y}_{lm}(\theta, \phi) + v_{ilm} \mathbf{Z}_{lm}(\theta, \phi)] , \quad (5)$$

where $\mathbf{Y}_{lm}(\theta, \phi)$ and $\mathbf{Z}_{lm}(\theta, \phi)$ are vector spherical harmonics (VSHs) [15]. Since (i) the VSHs represent the angular spectrum of VMFs [15] similarly to Eq. (4) and (ii) VSLMFs are defined as a linear combination of the VMFs according to Eq. (2), the same expansion coefficients u_{ilm} and v_{ilm} appear in Eq. (5) as in Eq. (2). Furthermore, following from the linearity of our expressions, the combination

$$\mathbf{A}(\theta_s, \phi_s) = \sum_m \sum_{i=1}^{i_{\max}} c_{mi} \mathbf{U}_{mi}(\theta_s, \phi_s) \quad (6)$$

of VSHs with the coefficients c_{mi} of Eq. (1) gives the angular spectrum $\mathbf{A}(\theta_s, \phi_s)$ of the focused field. The electric field at the entrance pupil of the lens can then be found using the vectorial ray-tracing method of Török et al. [16].

Although Eq. (4) resembles the Debye–Wolf integral [5] closely, it is important to stress that the integration is performed over the unit sphere of all possible plane-wave directions, not just for the spherical cap

$$S_C := \{(\theta_s, \phi_s) | 0 \leq \theta_s \leq \sin^{-1}(\text{NA}), 0 \leq \phi_s < 2\pi\}. \quad (7)$$

To be applicable to systems whose NA restricts possible plane-wave directions to S_C , the VSLHs $\mathbf{U}_{mi}(\theta, \phi)$ were constructed to maximize η_{mi} , the fraction of the energy falling onto S_C [15]. The VSLHs $\mathbf{U}_{mi}(\theta, \phi)$ for a given m are ordered by decreasing

η_{mi} , thus those with lower i have less “energy leakage” outside S_C . In our examples, we restrict ourselves to basis functions with $\eta_{mi} \gtrsim 98\%$. This leads to choosing the maximal index i_{\max} to be less than N_m . Hence, no extra constraints are necessary to ensure the directionality of the illumination, which would be inevitable when using the multipole theory of focusing [6].

3. The inverse problem

Next we demonstrate how to treat the inverse problem of finding the illumination for a prescribed focal intensity profile using the vector Slepian bases. Here we only consider examples of cylindrical vector beams that can be described as a superposition of radially and azimuthally polarized fields. In the context of VSLHs this means a choice of $m = 0$ [15]. However, all optimization tasks could be performed in a straightforward way for linear, circular or more general polarization states as well, merely involving different choices of m . Naturally, our method is easily applicable to inverse problems on the electric field distribution, too, provided that a physically feasible focal electric field is prescribed.

In our calculations an aplanatic lens with NA = 0.95 was used. Assuming a cylindrical coordinate system (ρ, φ, z) centered at the focus, a rotationally symmetric intensity distribution $I(\rho, z)$ was prescribed in the focal volume.

The focused field can be written as

$$\mathbf{E}(\mathbf{r}; c_i) = \sum_{i=1}^{i_{\max}} c_i \Phi_{0i}(\mathbf{r}), \quad (8)$$

where the task is to find the coefficients c_i that minimize the cost function

$$F(c_i) := \iiint_V [\mathbf{E}^*(\mathbf{r}; c_i) \cdot \mathbf{E}(\mathbf{r}; c_i) - I(\mathbf{r})]^2 d^3\mathbf{r}, \quad (9)$$

the squared error of the intensity integrated over some reasonably chosen volume V around the focus (the asterisk denotes the complex conjugate and we have simplified notation by omitting the zero m index from c_{0i}).

The optimization was performed by sequential least squares programming [17]. Random initial values of c_i were chosen and the process converged to a local minimum of $F(c_i)$. For a given problem, this optimization process was repeated 40 times and the lowest minimum was selected. Although not guaranteed to find a global optimum, the process yielded satisfactory results from a practical point of view. For the examples presented in this paper, real values of c_i are only considered. Complex-valued c_i , while increasing the computational complexity and rendering fabrication more difficult, did not yield better optima.

The angular spectrum of $\mathbf{E}(\mathbf{r})$ can be obtained as

$$\mathbf{A}(\theta_s, \phi_s) = \sum_{i=1}^{i_{\max}} c_i \mathbf{U}_{0i}(\theta_s, \phi_s). \quad (10)$$

Since $\eta_{mi} < 1$ [15], a small amount of energy leakage may still occur outside S_C . Because of that, the exact focused electric

fields were also calculated by Debye–Wolf integration using Chirp Z-Transform [18] after enforcing a hard limit at the edge of the entrance pupil.

The prescribed focal intensity functions for the needle, tube and bubble were

$$I(\rho) \propto \exp\left(-\frac{\rho^2}{a^2}\right), \quad (11a)$$

$$I(\rho) \propto \frac{\rho^2}{a^2} \exp\left(-\frac{\rho^2}{a^2}\right), \quad (11b)$$

$$I(\rho, z) \propto \frac{\rho^2 + (z/3)^2}{a^2} \exp\left[-\frac{\rho^2 + (z/3)^2}{a^2}\right], \quad (11c)$$

respectively, where the parameter a was chosen such that the full width at half maximum (FWHM) of all functions in the focal plane was 0.4λ . For the optical tube and bubble this value refers to the inner FWHM size of the dark spot. For the optical bubble, a physically feasible aspect ratio $\text{FWHM}_z/\text{FWHM}_\rho = 3$ was chosen, as seen in Eq. (11c). The integration in Eq. (9) was performed over a cylinder with a length of 10λ and a radius of 2λ for the needle and the tube, and over a prolate ellipsoid of revolution with a length of 12λ and a radius of 2λ for the bubble.

For both the optical needle and tube, the 11 most concentrated $\Phi_{0i}(\mathbf{r})$ functions were used. For the needle we included only $\Phi_{0i}(\mathbf{r})$ corresponding to radially polarized illumination, because the azimuthally polarized components would only increase the lateral FWHM and would not contribute to the on-axis electric field. For analogous reasons, $\Phi_{0i}(\mathbf{r})$ corresponding to azimuthally polarized illumination were included for the optical tube. The bubble included both types of polarizations. Moreover, since the ideal optical bubble demands zero electric field in its center, we introduced the extra constraint $\mathbf{E}(\mathbf{r} = \mathbf{0}; c_i) = \mathbf{0}$ in the optimization process.

4. Results

Fig. 1 depicts the intensity distributions obtained from the optimization processes for each spot with Fig. 2 showing the corresponding electric fields at the entrance pupil of the lens. In the case of the needle (Figs. 1(a),(b)), the length of the spot is 9.17λ (axial full width at 90% maximum), while the lateral FWHM is 0.41λ in the focal plane and below 0.44λ throughout its full length. The beam purity (expressing the fraction of energy of the longitudinally polarized component inside the needle volume, defined in Ref. [13]) stays above 80% along the needle with a value of 86% in the focal plane. Hence, we can conclude that the quality of the needle resulting from our method is comparable to that of Wang et al. [13]. Fig. 1(b) shows a slight difference between the Slepian approximation of the focused field using the VSLMFs $\Phi_{0i}(\mathbf{r})$ and the result of the Debye–Wolf integration. This discrepancy can be attributed to the fact that 0.54% of the total energy leaked outside the spherical cap of illumination.

The optical tube shown in Figs. 1(c),(d) has a length of 9.16λ , measured along $\rho = \rho_{\max}$, where ρ_{\max} is the peak radius in

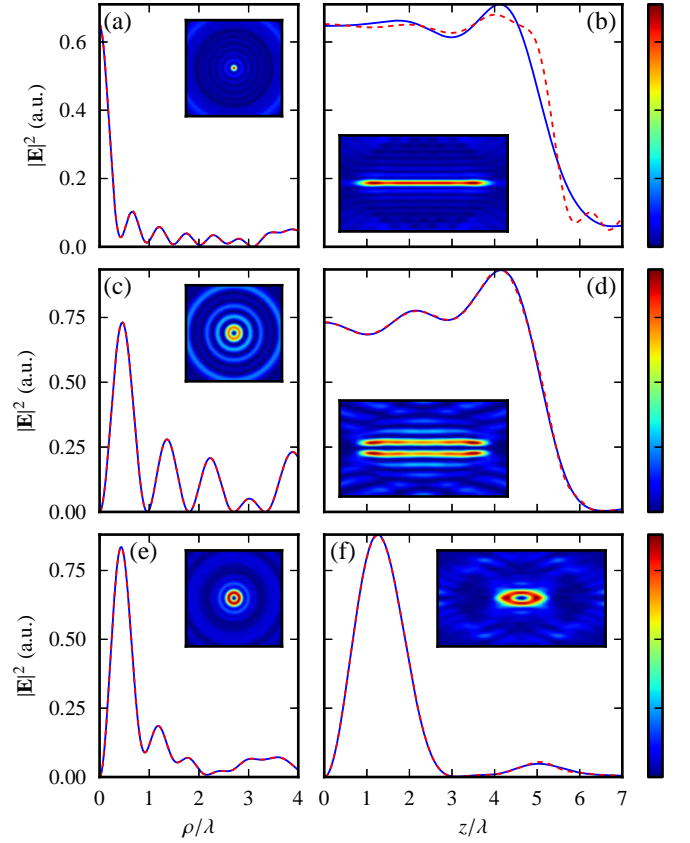


Figure 1: Radial and axial intensity cross-sections of the optical (a)-(b) needle, (c)-(d) tube and (e)-(f) bubble, respectively, with the solid line showing the result of the Debye–Wolf integration and the dashed line the VSLMF approximation (everywhere except in (b) the two curves practically overlap). The insets of show intensity contour maps in (a), (c), (e) the focal plane and (b), (d), (f) the meridional plane, respectively.

the focal plane; the lateral inner FWHM is 0.46λ in the focal plane and stays below 0.50λ throughout the entire length of the tube. Again, our results are comparable with those of Wang et al. [14]. Here the energy leakage is only 0.04% when using the Slepian approximation since the illumination intensity is low near the edge of the entrance pupil, as seen in Fig. 2(b).

We note that both for the optical needle and the tube, the maximal length attainable by the optimization depends on the number of basis functions involved in the process which itself depends on the maximal degree L of the VMFs and VSHs used for the construction of the VSLMF and VSLH bases [15]. For all examples presented here, we chose $L = 30$. By increasing L , the number of total VSLHs increases, including the number of those with $\eta_{mi} \approx 1$. While more optimization parameters are introduced, the maximal attainable length of the tube and needle also increases. Thus when increased depth of field is of primary importance, a larger value for L can simply be chosen.

Finally, the optical bubble of Figs. 1(e),(f) qualitatively reproduces the result of Bokor and Davidson [4]. In this case, the illumination (Fig. 2(c)) is constructed from 22 basis functions. The axial and lateral FWHM of the dark core of the bubble are 1.23λ and 0.43λ , respectively. As seen in Figs. 1(e),(f), the

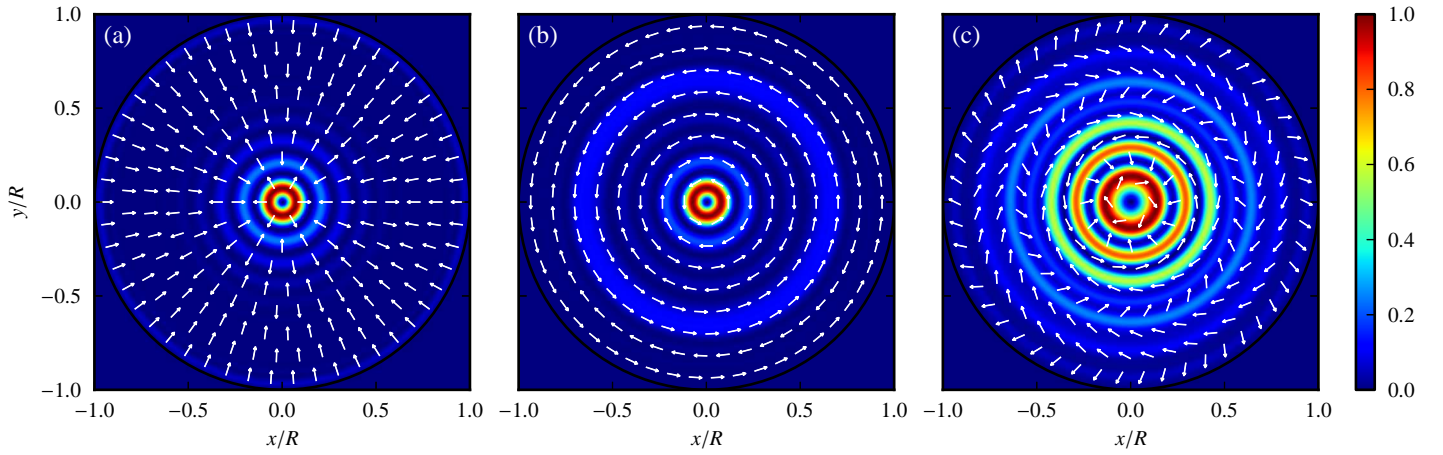


Figure 2: The intensity distribution and polarization of the electric field at the entrance pupil for the optical (a) needle, (b) tube, and (c) bubble (R is the radius of the entrance pupil).

intensity is zero at the center as prescribed, and the axial and transverse peak intensities are nearly equal in magnitude, which is advantageous e.g. in fluorescence depletion microscopy [4]. Again, the illumination intensity is low near the edge of the entrance pupil, leading to an energy leakage of only 0.06%.

5. Concluding remarks

We have demonstrated with three well-known examples that vector Slepian basis functions are highly suitable for the inverse problem of high NA focusing. Knowing the desired 3D intensity distribution in the focal volume, our method can be used effectively to design the electric field distribution at the entrance pupil.

Although the realization of the input field requires careful control of amplitude, phase and polarization, some practical methods involving liquid crystal spatial light modulators or form-birefringent spatially variant subwavelength gratings have already been proposed to achieve this task [19–21].

Finally, it is important to note again that our Slepian bases are suitable for treating the inverse problem not only for the focal intensity but for the focal electric field as well.

Acknowledgments

This work is connected to the scientific program of the “Development of quality-oriented and harmonized R+D+I strategy and functional model at BME” project. This project is supported by the New Hungary Development Plan (Project ID: TÁMOP-4.2.1/B-09/1/KMR-2010-0002).

References

- [1] Y. Zhao, Q. Zhan, Y. Zhang, Y. Li, Creation of a three-dimensional optical chain for controllable particle delivery, *Opt. Lett.* 30 (8) (2005) 848–850. doi:10.1364/OL.30.000848.
- [2] W. Chen, Q. Zhan, Three-dimensional focus shaping with cylindrical vector beams, *Opt. Commun.* 265 (2) (2006) 411–417. doi:10.1016/j.optcom.2006.04.066.
- [3] T. Jabbour, S. Kuebler, Vector diffraction analysis of high numerical aperture focused beams modified by two- and three-zone annular multi-phase plates, *Opt. Express* 14 (3) (2006) 1033–1043. doi:10.1364/OE.14.001033.
- [4] Bokor, N. and Davidson, N., A three dimensional dark focal spot uniformly surrounded by light, *Opt. Commun.* 279 (2) (2007) 229–234. doi:10.1016/j.optcom.2007.07.014.
- [5] E. Wolf, Electromagnetic Diffraction in Optical Systems. I. An Integral Representation of the Image Field, *P. Roy. Soc. A - Math. Phys.* 253 (1274) (1959) 349–357. doi:10.1098/rspa.1959.0199.
- [6] C. Sheppard, P. Török, Efficient calculation of electromagnetic diffraction in optical systems using a multipole expansion, *J. Mod. Optics* 44 (4) (1997) 803–818. doi:10.1080/09500349708230696.
- [7] R. Kant, An analytical solution of vector diffraction for focusing optical systems, *J. Mod. Optics* 40 (2) (1993) 337–347. doi:10.1080/09500349314550341.
- [8] J. Braat, P. Dirksen, A. Janssen, A. van de Nes, Extended Nijboer–Zernike representation of the vector field in the focal region of an aberrated high-aperture optical system, *J. Opt. Soc. Am. A* 20 (12) (2003) 2281–2292. doi:10.1364/JOSAA.20.002281.
- [9] S. Sherif, M. Foreman, P. Török, Eigenfunction expansion of the electric fields in the focal region of a high numerical aperture focusing system, *Opt. Express* 16 (5) (2008) 3397–3407. doi:10.1364/OE.16.003397.
- [10] R. Kant, Superresolution and increased depth of focus: an inverse problem of vector diffraction, *J. Mod. Opt.* 47 (5) (2000) 905–916. doi:10.1080/09500340008235099.
- [11] J. Braat, P. Dirksen, A. Janssen, S. van Haver, A. van de Nes, Extended Nijboer–Zernike approach to aberration and birefringence retrieval in a high-numerical-aperture optical system, *J. Opt. Soc. Am. A* 22 (12) (2005) 2635–2650. doi:10.1364/JOSAA.22.002635.
- [12] M. Foreman, S. Sherif, P. Munro, P. Török, Inversion of the Debye–Wolf diffraction integral using an eigenfunction representation of the electric fields in the focal region, *Opt. Express* 16 (7) (2008) 4901–4917. doi:10.1364/OE.16.004901.
- [13] J. Wang, W. Chen, Q. Zhan, Engineering of high purity ultra-long optical needle field through reversing the electric dipole array radiation, *Opt. Express* 18 (21) (2010) 21965–21972. doi:10.1364/OE.18.021965.
- [14] J. Wang, W. Chen, Q. Zhan, Three-dimensional focus engineering using dipole array radiation pattern, *Opt. Commun.* 284 (2011) 2668–2671. doi:10.1016/j.optcom.2011.02.030.
- [15] K. Jahn, N. Bokor, Vector Slepian basis functions with optimal energy concentration in high numerical aperture focusing, *Opt. Commun.* 285 (2012) 2028–2038. doi:10.1016/j.optcom.2011.11.107.
- [16] P. Török, P. Munro, E. Kriezis, High numerical aperture vectorial imaging in coherent optical microscopes, *Opt. Express* 16 (2) (2008) 507–523. doi:10.1364/OE.16.000507.
- [17] D. Kraft, A software package for sequential quadratic programming,

Tech. Rep. DFVLR-FB 88-28, DLR German Aerospace Center – Institute for Flight Mechanics, Köln, Germany (1988).

- [18] K. Jahn, N. Bokor, Intensity control of the focal spot by vectorial beam shaping, *Opt. Commun.* 283 (2010) 4859–4865. doi:10.1016/j.optcom.2010.07.030.
- [19] X. Wang, J. Ding, W. Ni, C. Guo, H. Wang, Generation of arbitrary vector beams with a spatial light modulator and a common path interferometric arrangement, *Opt. Lett.* 32 (24) (2007) 3549–3551. doi:10.1364/OL.32.003549.
- [20] W. Chen, Q. Zhan, Diffraction limited focusing with controllable arbitrary three-dimensional polarization, *J. Opt.* 12 (2010) 045707. doi:10.1088/2040-8978/12/4/045707.
- [21] U. Levy, C. Tsai, L. Pang, Y. Fainman, Engineering space-variant inhomogeneous media for polarization control, *Opt. Lett.* 29 (15) (2004) 1718–1720. doi:10.1364/OL.29.001718.